Molten Carbonates Electrolyzer Model for Hydrogen Production Coupled to Medium/Low Temperature Solar Power Plant

Miguel A. Reyes-Belmonte[1], Alfonso Delgado[2], Elena Díaz[1], José González-Aguilar[1] and Manuel Romero[1]

[1] IMDEA Energy Institute, Móstoles (Spain)

[2] Universidad Autónoma de Madrid, Madrid (Spain)

Abstract

In this work, mathematical model of molten carbonates electrolyzer (MCEC) has been developed for its integration into concentrating solar power (CSP) plant. MCEC modeling has been based on electrochemical and thermodynamics approach using experimental information from a testing device. Despite the high temperature requirements for MCEC operation (above 500 ℃), heat generation during the electrolysis process reduces the requirement of external heat addition. Energy optimization approach using ASPEN HYSYS pointed out that MCEC stable operation could be achieved for a wide temperature range of the feeding steam by using smart heat recovery diagram. Temperature conditions that are covering from exothermal to thermoneutral working conditions have been explored depending on the input thermal and electrical requirements. MCEC model described in this work has been encoded into TRNSYS platform for transient performance evaluation. Optimal integration scheme of MCEC coupled to linear-Fresnel solar plant has been proposed and sized for the hydrogen production of a refueling station.

Keywords: High Temperature Electrolysis, Molten Carbonates, CSP Modeling, Hydrogen Production

1. Introduction

Concentrating Solar Power (CSP) consists in producing electricity through thermo-mechanical transformation by heating a working fluid using concentrating solar technologies (parabolic through, solar tower, parabolic dish or linear Fresnel (Lovegrove and Stein, 2012)). Later this fluid is expanded inside the turbine of a power cycle converting the thermal energy into mechanical power and electricity by its self-mounted generator. CSP deployment has been growing over the last few years as it is seen as one of the most promising energy options for the upcoming years. This is mainly due to its high flexibility on energy dispatch thanks to use of thermal energy storage (TES).

Apart from the wide variety of TES systems mainly focused on short- medium term thermal storage, an alternative way is considered based on production of energy carriers like hydrogen. In this case, hydrogen can be used either for compressed storage, transportation, electricity production using a fuel cell (Carrette et al., 2001), engine powering (Dimitriou and Tsujimura, 2017) or as a valuable product for chemical and oil companies. Despite the high interest and number of applications for hydrogen, its production is still considered a costly and high greenhouse gas emission process since most of hydrogen is still produced from fossil fuel sources. However, for becoming a true zero-emission energy carrier, hydrogen should be produced from renewable energy sources such as wind, solar energy (Sanz-Bermejo et al., 2014b) or biomass (Dincer and Acar, 2015). Several technologies can be used for hydrogen production from renewable energy sources such as biomass gasification, solar-driven direct water splitting, solar-driven high-temperature thermochemical water splitting, bio-derived liquids reforming or water electrolysis using renewable electricity (Ibrahim Dincer, 2012). Water electrolysis is based on water splitting into its components (hydrogen and oxygen) inside an electrochemical device (electrolyzer) by applying an electrical current. Low temperature water electrolysis is a mature technology and hydrogen plants based on alkaline or proton exchange membrane (PEM) electrolyzers are very common. Nevertheless, power consumption is relatively high (Zeng and Zhang, 2009). Therefore high temperature steam electrolysis is being developed as an alternative because it shows a decrease on the electrical power requirements in spite of an increase of thermal energy demands as steam temperature increases (Laurencin and Mougin, 2015). This is explained from kinetics point of view, since higher temperature is promoting electrode activity while reducing cell overvoltage what is translated into lower energy losses and

doi:10.18086/swc.2017.04.13 Available at http://proceedings.ises.org

more efficient process (Schiller et al., 2009). Two main electrolyzer technologies can be distinguished for high temperature electrolysis; these are Solid Oxide Electrolytic Cell (SOEC) and Molten Carbonates Electrolytic Cell (MCEC). These devices operate at temperatures above 500 ℃ at higher power density than conventional low temperature electrolyzers. These characteristics allow more compact components and less number of units. SOEC and MCEC can work either as electrolyzer or as fuel cells improving grid stabilization in a near and likely future with high penetration of renewable energy sources.

In this work, an electrochemical and thermodynamic model for molten carbonates electrolyzer (MCEC) has been developed and validated with experiments from small lab demo prototype (Frangini et al., 2014). Due to the small size prototype, scaling-up design has been proposed and applied for larger power plants corresponding to commercial application of 400 kg/day for hydrogen production. This scenario corresponds to hydrogen requirements for municipality refueling station (Sanz-Bermejo et al., 2014a). Proposed model has been used to investigate the effect of working operative conditions (current density, steam temperature, conversion ratio…) on MCEC performance. Trends and limits found from that analysis will help choosing best operative conditions. Later, proposed model has been encoded as a TRNSYS component (Trnsys, 2007) for the dynamic analysis. Integration scheme for MCEC coupling to the solar plant has been proposed and energy recovery network optimized for system efficiency maximizing. Finally, solar plant requirements have been discussed for linear Fresnel coupling assessment.

2. Molten carbonates electrolyzer (MCEC) description

One of the main differences between SOEC electrolyzers and MCEC is the requirements of the second one on CO_2 feeding together with water steam. Water and carbon dioxide molecules decompose into H_2 and carbonate ion (CO^{3-}) at electrolyzer cathode. Simultaneously CO_3^{2-} diffusion occurs through the alkaline electrolyte made of lithium, sodium and potassium towards the anode resulting into CO_2 and O_2 (Hu et al., 2014). Chemical reactions occurring inside the MCEC are summarized in Table 1.

Table 1 MCEC involved reactions

Cathode	$H_2O + CO_2 + 2e^- \leftrightarrow H_2 + CO_3^{2-}$
Anode	$CO_3^{2-} \leftrightarrow CO_2 + ½\ O_2 + 2e^-$
Full conversion	$H_2O + O_2 \leftrightarrow H_2 + CO_2 + ½\ O_2$
ΔH_r (298 K)	285,8 kJ/mol

Nickel-based alloy with chromium and aluminum rate between 2-10 % is employed for the cathode due to its sintering resistance and mechanical properties (Bodén, 2007). The anode is made of NiO with lithium and MgO intercalated (Antolini, 2011; Hu et al., 2014) in order to avoid short-circuits into the cathode. Ceramic matrix made of $LiAlO_2$ (Hu et al., 2014) separates the cathode from the anode and supports the electrolyte LiNaK, which is a ternary eutectic mixture of molten carbonates Li_2CO_3-Na_2CO_3-K_2CO_3 (Frangini et al., 2014; Hu et al., 2014).

MCE concept is quite flexible and apart from H_2 and O_2 production as it is discussed in this work, it could operate for oxy-fuel combustion processes or methanation as it can be observed from Figure 1.

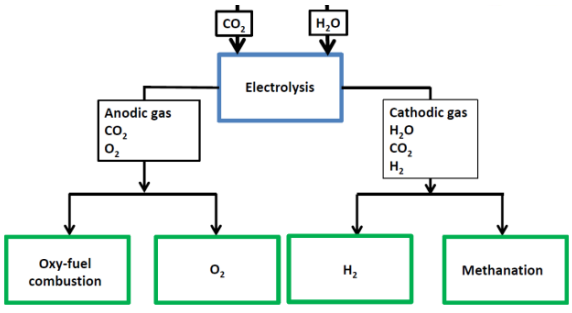

Figure 1 Applications of MCEC electrolyzer

2.1 Experimental device

Small lab-scale MCE was designed, developed and tested by ENEA (Frangini et al., 2014). This electrolyzer was made of a gold electrode with surface area of 0.2 cm^2 and a standard oxygen electrode of gold immersed in molten electrolyte and hold by alumina tube with a small hole at the bottom part. CO_2 and O_2 mixture in a relation of 2:1 with gold sheet of 1cm^2 surface was employed as counter-electrode. A mixture composed of alkaline molten carbonates Li_2CO_3-Na_2CO_3-K_2CO_3 with 43.5-31.5-25.0% molar ratio was used. This mixture has its melting point at 397 ℃. Several steady-state galvanostatic and cyclic voltammetric tests were performed for a temperature range between 500 ℃ and 600 ℃ as it can be seen on Figure 2. Experiments were performed by introducing different gas compositions of dry CO_2 and wet mixture in a 50:50 composition (p_{CO2}=0.5 atm; p_{H2O} =0.5 atm) at 120 ℃ with a flow rate of 60 mL/min (Frangini et al., 2014).

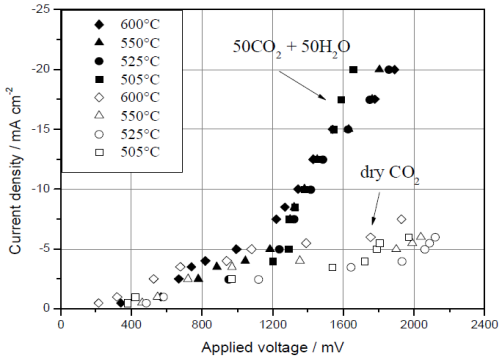

Figure 2 Applied voltage dependency according to experimental results at different temperatures (Frangini et al., 2014)

3. Mathematical model

MCE model was based on the electrochemical equations shown below.

3.1 Potential calculation: Nerst, reversible and thermoneutral

Reversible potential exchanged in a cell (eq. 1) depends on Gibbs free energy that changes with cell temperature *T* according to (eq. 2) (Brouwer et al., 2006; Petipas et al., 2013)

$$E_{REV} = \frac{\Delta_r G_T^0}{2 \cdot F} \qquad \text{(eq. 1)}$$

Where *F* is the Faraday's constant equal to 96485.33 C mol^{-1}.

$$\Delta_r G_T^0 = 244800 - 49.18 \cdot T - 2.72 \cdot 10^{-3} \cdot T^2 \qquad \text{(eq. 2)}$$

Nernst potential (eq. 3) depends on gases partial pressure in cathode and anode, according to electrolyzer operating pressure and spices composition (Brouwer et al., 2006).

$$E_N = E_{REV} + \frac{R \cdot T}{2 \cdot F} ln\left[\frac{p_{H_2,cat} \cdot p_{O_2,an}^{1/2} \cdot p_{CO_2,an}}{p_{H_2O,cat} \cdot p_{CO_2,cat}}\right] \qquad \text{(eq. 3)}$$

Thermoneutral potential can be derived from (eq. 4)

$$E_{TN} = \frac{\Delta_r H_T}{2 \cdot F} \qquad \text{(eq. 4)}$$

Where $\Delta_r H_T$ is the reaction enthalpy (eq. 5) given by (Petipas et al., 2013).

$$\Delta_r H_T = 238200 + 13.12 \cdot T - 3.53 \cdot 10^{-3} \cdot T^2 \qquad \text{(eq. 5)}$$

3.2 Mass balance

Streams flow and composition can be determined using the following mass balance equations (eq. 6-10). On the first hand, hydrogen molar flow can be estimated according to Faraday's electrolysis law (eq. 6) (Petipas et al.,

2013).

$$n_{H2} = \frac{j \cdot S}{2 \cdot F} \quad \text{(eq. 6)}$$

Hydrogen production is proportional to current density j (A/cm^2) and electrodes active surface S (cm^2). Once hydrogen molar production has been determined, composition of involved species in the cathode can be determined by taking the standard conversion steam rate of the cell (x_{H2O}). Molar flow for cell feeding (n_{H2O}) can be calculated from (eq. 7).

$$n_{H_2O,cat} = \frac{n_{H_2}}{x_{H_2O}} \quad \text{(eq. 7)}$$

Considering that cell feeding is equimolar (0.5 H_2O + 0.5 CO_2) (eq. 8) can be derived (Frangini et al., 2014).

$$n_{CO_2,cat} = n_{H_2O,cat} \quad \text{(eq. 8)}$$

In a similar way, mass balance applied to electrolyzer anode results into (eq. 9) and (eq. 10).

$$n_{O2,an} = n_{H2}\, 0.5 \quad \text{(eq. 9)}$$

$$n_{CO2,an} = n_{H2} \quad \text{(eq. 10)}$$

3.3 Overpotential calculation

Electrolyzer working potential (E) can be determined as the sum of all system irreversibilities (eq. 11) (Brouwer et al., 2006) and includes ohmic losses (E_{ohm}), activation overpotential (η) and Nernst potential (E_N).

$$E = E_N + E_{ohm} + \eta(j) \quad \text{(eq. 11)}$$

Ohmic losses can be determined from Ohm law while the overpotential (η) is determined from Butler-Volmer expression (eq. 12) (Brouwer et al., 2006).

$$\eta = \frac{R \cdot T}{2 \cdot \alpha_A \cdot F} \cdot \sinh^{-1} \cdot \left(\frac{j}{2 \cdot j_{0,an} \cdot S} \right) + \frac{R \cdot T}{2 \cdot \alpha_C \cdot F} \cdot \sinh^{-1} \cdot \left(\frac{j}{2 \cdot j_{0,cat} \cdot S} \right) \quad \text{(eq. 12)}$$

Where j is the exchanged current (A/cm^2), α_c, α_A are transfer coefficients for cathode and anode while $j_{0,an}$ and $j_{0,cat}$ are the exchange currents of anode and cathode respectively. Due to the complexity on parameters fitting from Butler-Volmer equation and its later model programming (Sanz-Bermejo et al., 2015) simplified (eq. 13) has been proposed (Ulleberg, 2003) instead of (eq. 11).

$$E = E_{REV} + r \cdot j + s \cdot \log_{10}(t \cdot j + 1) \quad \text{(eq. 13)}$$

Where r, s and t parameters are referring to the ohmic resistance (r) and electrolyzer overpotential (s, t) that are depending on temperature.

3.4 Applied power

Electrical applied power (P) can be determined multiplying cell voltage (E), current density (j), surface (S) and the number of cells (N).

$$P = j \cdot N \cdot E \cdot S \quad \text{(eq. 14)}$$

3.5 Cell geometry

Cell dimensioning was addressed according to the following equations and considering that cells were arranged in a stack (Petipas et al., 2013; Yu et al., 2007). Unit volume depends on cell length (l), cell thickness (e_{cell}), endplate thickness (e_{plate}) and the number of cells (N) (eq. 15).

$$V = l^2 \cdot \left(N \cdot e_{cell} + 2 \cdot e_{plate} \right) \quad \text{(eq. 15)}$$

Number of stacks (eq. 16) are depending on unit volume and length.

$$N_{stack} \approx \left(\frac{\sqrt[3]{V}}{l} \right) \quad \text{(eq. 16)}$$

Number of cells per stack ($N_{cell/stack}$) can be calculated dividing the number of cells (N_{cell}) and stacks (N_{stack}). From abovementioned parameters, unit surface (S_{unit}) can be determined from (eq. 17).

$$S_{unit} = 4 \cdot \left(N_{stack} \right)^{1/2} \cdot l \cdot \left(N_{cell/stack} \cdot e_{cell} + 2 \cdot e_{endplate} \right) + 2 \cdot N_{stack} \cdot l^2 \quad \text{(eq. 17)}$$

3.6 Energy balance

Energy balance for the electrolyzer can be expressed according to (eq. 18).

$$K_s \cdot \frac{dT}{dt} = E \cdot j \cdot S \cdot (1 - \eta) - \frac{(T - 25)}{R} - n_{H_2O} \cdot c_{p_{H_2O}} (T - T_{IN}) - n_{CO_2} \cdot c_{p_{CO_2}} (T - T_{IN}) \quad \text{(eq. 18)}$$

Left-hand side of the equation accounts for the temperature variation of the electrolyte whose thermal capacity was already characterized (An et al., 2016). On the right-hand side of the expression, the first term represents the gained thermal energy while the other terms are representing the energy losses. T is referring to the cell temperature while T_{IN} corresponds to the feeding temperature. Cell efficiency is determined as the ratio between thermoneutral potential (E_{TN}) and total potential (E).

3.7 Iterative solving method

MCE electrolyzer model has been derived from standard electrochemical and thermodynamics equations that are solved following the flow diagram presented on Figure 3. Design input parameters such as cell current density and steam conversion are needed for electrolyzer modeling, these parameters can be estimated from lessons learnt during experimental testing device (Frangini et al., 2014). Steam flowrate required for the electrolysis process was determined accordingly to the chosen conversion and desired hydrogen production. Main design criteria for MCE was based on hydrogen production rates for its later application, while from modeling results the number of cells, stack geometry, electricity consumption, production rates (CO_2, H_2, steam), cell temperature and the thermal energy released will be determined by solving material and energy balance equations (Petipas et al., 2013; Ulleberg, 2003).

3.8 Model fitting

Proposed model for MCEC has been calibrated using experimental data shown in Figure 2 what resulted into a series of fitting parameters for *r*, *s* and *t* (eq. 13). Family of coefficients was obtained due to temperature dependence of *r* and *t.* This allowed temperature-based equations definition shown in Table 2.

Table 2 Fitting coefficients proposal

Parameter	Value
r (Ω cm^2)	$-7.58 \cdot 10^{-5} \cdot T + 8.19 \cdot 10^{-2}$
s (V)	$2{,}18 \cdot 10^{-2}$
t (cm^2/mA)	$-5.69 \cdot 10^{-8} \cdot T + 6.62 \cdot 10^{-5} \cdot T - 1.91 \cdot 10^{-2}$

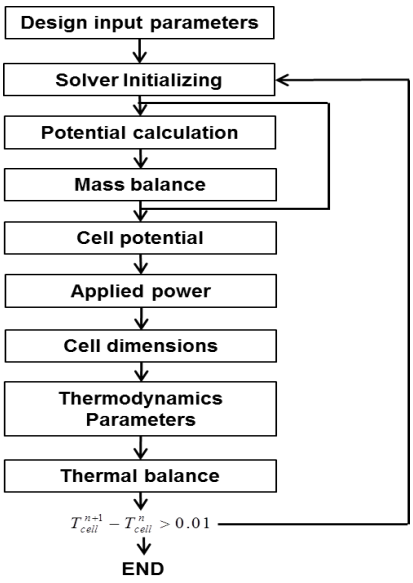

Figure 3 Solving diagram for MCEC characterization

4. Sensitivity analysis

MCEC performance has been explored using the model described above. Effects of conversion ratio, current density and feeding temperature on cell temperature and electrical power have been investigated by means of the sensitivity analysis shown on Figure 4. Data were obtained for 400 kg/day production of H_2 by fixing feeding temperature at 100 ℃ (when not modified) and 60% conversion (when not modified).

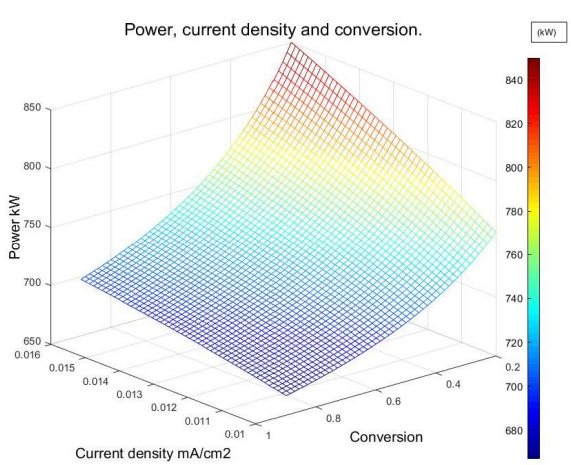

a. Given feeding temperature (100 ℃)

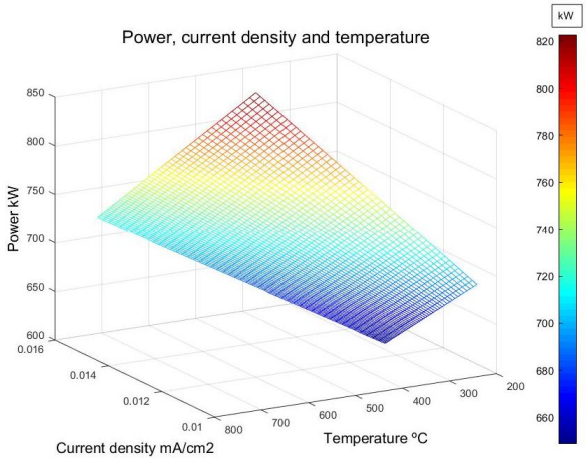

b. Given conversion rate (60%)

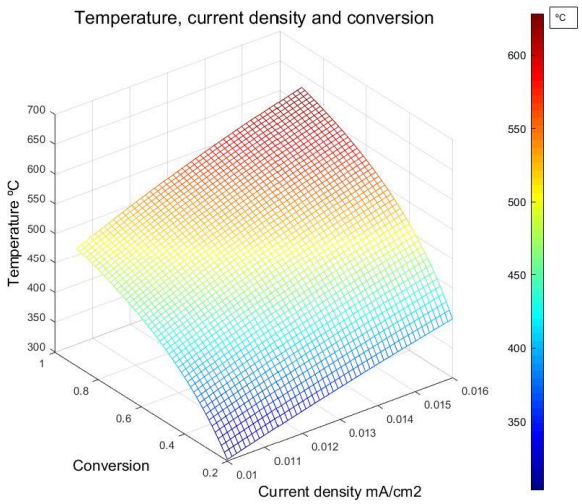

c. Given feeding temperature (100 ℃)

Figure 4 Working conditions effect on MCEC performance. Power consumption (top). Cell temperature (bottom)

As it can be observed from Figure 4-a, higher conversion rates and lower energy density currents would be desired in order to reduce electrical power consumption of the electrolyzer. Those conditions correspond to intermediate cell temperature range (400 ℃ – 500 ℃) as it can be observed from Figure 4-c. This figure also gives an idea about the working range for the electrolyzer, since lowest cell temperature is limited to 400 ℃ to avoid molten carbonates electrolyte freezing. Figure 4-b shows the effect of MCE feeding temperature (steam and CO_2) into electrical power consumption for a given conversion rate. As it can be observed, the lower is the feeding temperature of streams, the higher is the electrical power consumption for the electrolysis process. In other words, higher thermal input energy will be compensated with lower electrical power consumption of the electrolyzer which is the design target. Optimum working conditions for the electrolyzer should meet low density currents, with high conversion rates and high feeding temperatures.

5. Plant integration

As it was observed on Figure 4-b, high temperatures of the feeding streams to the electrolyzer are desired due to the lower electrical power consumption. In addition, MCE can operate under exothermal conditions which are increasing the temperature of the electrolyte cell. Thermal energy generated during the exothermal process can be mostly recovered using a heat exchangers network; the objective of this regeneration process is two-fold. On the one hand, it would increase the temperature of feeding streams (steam and CO_2) what will reduce electric power consumption of the MCEC. On the other hand, hot streams out of the electrolyzer will be cooled-down what is required for H_2 and O_2 separation processes whether using amines process or membranes.

Figure 5 shows the energy recovery network proposed for MCEC operation, this network was optimized using pinch-point methodology (Das, 2005) on ASPEN Energy Analyzer (AspenTech, 2017). This optimization was based on energy recovery maximizing from hot products streams (electrolyzer output) for input streams preheating (steam and CO_2) by using network of heat exchangers named as E-101, E-103, E-104, E-105 and E-106. Water from the network will be pumped into the system and firstly preheated by low temperature products stream at heat exchanger E-101. Later, water stream will be heated-up using external heat addition at E-102 in case of the electrolyzer operation cannot cover the thermal demand. This thermal power could be provided by external process heat as for example from concentrating solar power (CSP) plant. After external heat addition, heat exchanger network will be used for reaching the operation temperature of the electrolyzer. As it can be observed, membranes separation process (M-101 and M-102) has been proposed for CO_2 separation from products streams (H_2 + CO_2 for stream marked as 7 and O_2 + CO_2 for output stream 8). Separated CO_2 is recirculated back for electrolyzer feeding mixed with pumped water. Demister (component V-101) is considered for downstream cathode line for water droplets separation in those cases where the electrolyzer is operating with a conversion ratio lower than 100%. Condensed water is pumped back and mixed with feeding water stream. As

it can be observed, cathode stream (7) is cooled down while preheating feeding water through heat exchanger E-101; this will favor water droplets separation while reducing external heat addition on heat exchanger E-102. Furthermore, suitable temperature for membranes separation process M-101 will be expected after E-101 cooling down. Additional heat exchanger E-107 has been included as a heat sink for cooling down anode stream (8) to ensure low temperature for CO_2 separation on membrane M-102.

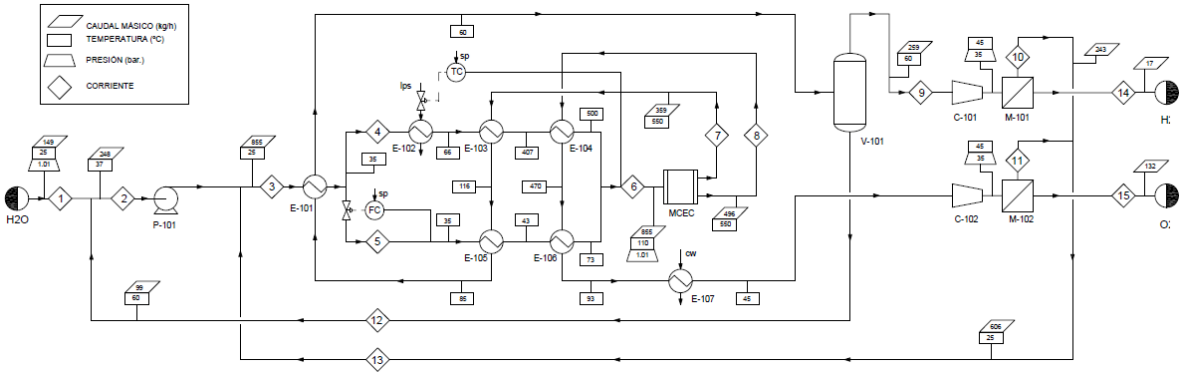

Figure 5 Energy recovery network of the MCEC

As it has can be observed on the diagram from Figure 5, feeding water stream mixed with CO_2 was separated into two streams (4 and 5) for optimizing preheating process what will reduce the external heat addition and optimizing heat exchangers network design. Mass flow splitting factor was optimized according to ASPEN HYSYS Energy Analyzer tool resulting into a ratio of 60% through the branch 4 and 40% trough branch 5 which optimized the annual cost of the system. Later, both streams were mixed again for electrolyzer feeding (branch 6). Electrolyzer feeding using separated branches was considered as well, but this option was discarded due to less efficient energy utilization resource according to pinch-point analysis.

6. TRNSYS integrated model

MCEC model described above has been programmed as a TRNSYS component (own created Type203) which will allow for performance evaluation under transient conditions and its coupling to a solar power plant. Mixer component numbered as Type210 was also developed to precisely account for energy balance when mixing streams with different fluids and with temperature dependent specific heat capacities.

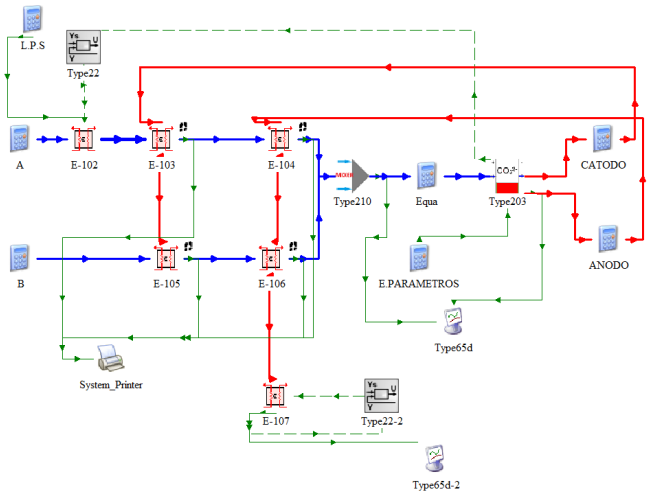

Figure 6 TRNSYS layout for MCEC developed model and auxiliaries

TRNSYS integrated model allowed to investigate the dynamic effect of warming-up the electrolyzer or its response to fluctuating temperature of feeding streams as it can be observed from Figure 7. Warming-up scenario is described on Figure 7-a, in this case the electrolyzer is fed at 1 bar and 100 ℃ while molten

carbonates electrolyte are kept at initial temperature of 400 ℃ (below that temperature will froze). As it can be observed, cell temperature will increase due to the exothermal electrolysis process till converging to 539 ℃ cell temperature. Electrical power reduction as cell temperature is increasing is observed based on kinetics improvement and reversible potential reduction (Mazloomi et al., 2012). Figure 7-b shows electrolyzer time response against a change on feeding temperature according to sinusoidal temperature oscillation. As it can be seen, amplitude signal of 50 ℃ on the feeding stream was dumped to less than 10 ℃ for the electrolyte due to its thermal capacity. Similar effect on the time delay of temperature signal for the electrolyzer cell was found when varying the feeding temperature.

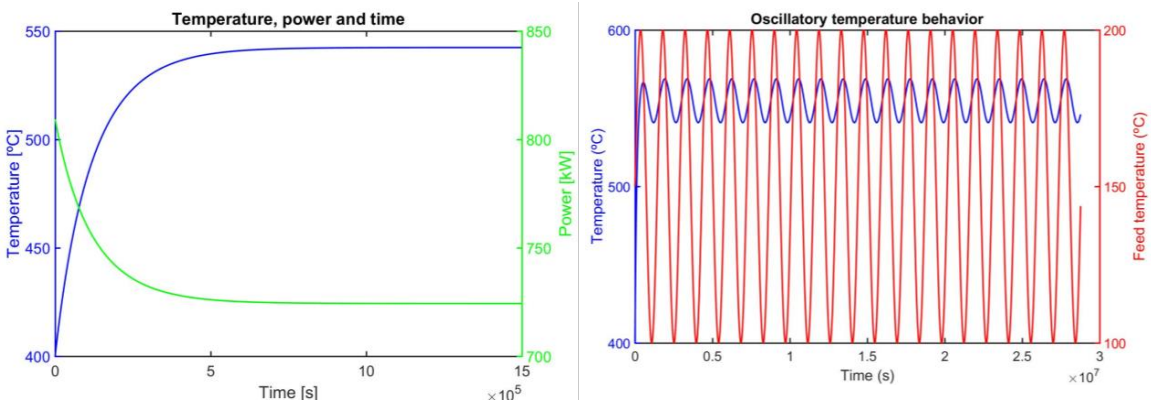

Figure 7 Time response of MCEC model programmed into TRNSYS. Electrolyzer warming-up (a). Fluctuating response (b)

7. Modelling results

Modelling results for commercial application using MCEC concept studied in this paper are presented on Table 3. Two different cases have been modelled, one corresponding to exothermal MCEC behavior with low feeding temperature and another one for thermoneutral working conditions. Working conditions for the exothermal case were taken from lessons learnt from experimental test data (Frangini et al., 2014), considering conversion ratio of 60% for current density of 0.014 A/cm^2 and low feeding temperature. Thermoneutral working conditions were determined from (eq. 4) considering cell temperature of 550 ℃. As it can be seen, the exothermal working mode consumes higher electrical power for the electrolysis process than thermoneutral mode (23% more). However, external thermal power requirements are one fourth of the thermoneutral needs at a lower temperature (40 kW at 110 ℃ instead of 160 kW at 550 ℃ from thermoneutral mode).

Table 3 Modelling results for commercial application

		Units	Exothermal	Thermoneutral
Assumptions	H_2 production	kg/day	400	400
	Current density	A/cm^2	0.014	0.0073
	Conversion rate	%	60	60
	Feeding temperature	℃	110	550
Model calculation	Cell temperature	℃	539	550
	Feeding steam	kg/h	248.2	248.2
	Feeding CO_2	kg/h	606.4	606.4
	Applied voltage	V	1.62	1.34
	Number of cells	-	319000	616000
	Electric power consumed	kW	726	593
	Required external thermal power	kW	40	160

According to results shown on Table 3, exothermal mode is suitable for low temperature applications since small amounts of thermal heat at low temperature are enough for hydrogen production using molten carbonates electrolyzer. For example, it could be coupled to low temperature CSP applications such as linear Fresnel collector according to diagram shown on Figure 8. In that case, dedicated linear Fresnel CSP plant is considered for external heat generation required for increasing temperature of feeding streams to the electrolyzer (heat exchanger named E-102 on Figure 5).

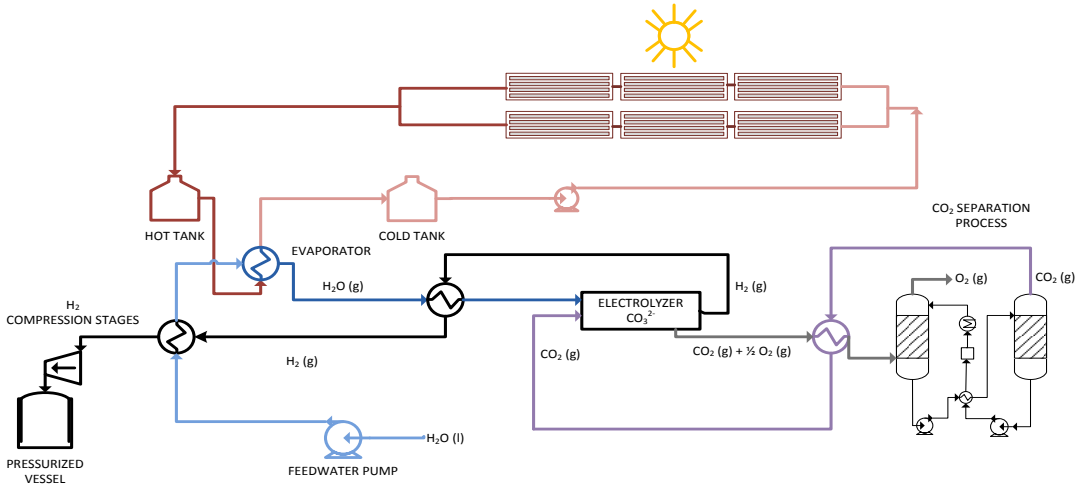

Figure 8 MCEC coupling to dedicated linear Fresnel CSP plant

8. Conclusions

In this paper it has been analyzed the application of molten carbonates electrolyzer cell (MCEC) for hydrogen production. Mathematical model has been developed based on electrochemical and thermodynamics equations and encoded as TRNSYS component for dynamic performance evaluation. MCEC model was completed considering experimental data from lab-scale demonstrator which also contributed to determine model assumptions (conversion ratio and operative cell temperatures). Sensitivity analysis performed on MCEC model demonstrated that operative conditions corresponding to high conversion ratios and low density currents were preferred due to the lower electricity requirements for the electrolysis process. However those conditions were leading to low cell temperatures what could damage the electrolyzer by freezing the electrolyte. It was also found that smart energy recovery network was required for input streams pre-heating for reducing external thermal power requirements, and in this case, splitting the mass flow into two streams (60% and 40%) will be beneficial according to pinch-point methodology. Dynamic response of TRNSYS model simulation showed how the electrolyzer was able to dump temperature fluctuations of the input streams while shifting its response due to molten carbonates thermal inertia.

9. Acknowledgments

The research leading to these results has received funding from EU FP7/2013-2017 under grant agreement n 609837 (FP7 IRP STAGE-STE). The authors would like to thank “Comunidad de Madrid” for its support to the ALCCONES project (S2013/MAE-2985) through the Program of R&D activities between research groups in Technologies 2103, co-financed by structural funds.

10. References

An, X., Cheng, J., Zhang, P., Tang, Z., Wang, J., 2016. Determination and evaluation of the thermophysical properties of an alkali carbonate eutectic molten salt. Faraday Discuss. 190, 327–338. doi:10.1039/C5FD00236B

Antolini, E., 2011. The stability of molten carbonate fuel cell electrodes: A review of recent improvements. Applied Energy 88, 4274–4293. doi:10.1016/j.apenergy.2011.07.009

AspenTech, 2017. Aspen HYSYS v8.8 [WWW Document]. AspenTech: Optimizing Process Manufacturing. URL http://www.aspentech.com/products/aspen-hysys/ (accessed 3.23.17).

Bodén, A., 2007. The anode and the electrolyte in the MCFC. KTH Chemical Science and Engineering.

Brouwer, J., Jabbari, F., Leal, E.M., Orr, T., 2006. Analysis of a molten carbonate fuel cell: Numerical modeling and experimental validation. Journal of Power Sources 158, 213–224. doi:10.1016/j.jpowsour.2005.07.093

Carrette, L., Friedrich, K.A., Stimming, U., 2001. Fuel Cells - Fundamentals and Applications, Fuel Cells. WILEY‐VCH Verlag GmbH. doi:10.1002/1615-6854(200105)1

Das, S.K., 2005. Process heat transfer. Alpha Science International, Harrow.

Dimitriou, P., Tsujimura, T., 2017. A review of hydrogen as a compression ignition engine fuel. International Journal of Hydrogen Energy 42, 24470–24486. doi:10.1016/j.ijhydene.2017.07.232

Dincer, I., Acar, C., 2015. Review and evaluation of hydrogen production methods for better sustainability. International Journal of Hydrogen Energy 40, 11094–11111. doi:10.1016/j.ijhydene.2014.12.035

Frangini, S., Felici, C., Tarquini, P., 2014. A Novel Process for Solar Hydrogen Production Based on Water Electrolysis in Alkali Molten Carbonates. ECS Transactions 61, 13–25. doi:10.1017/CBO9781107415324.004

Hu, L., Rexed, I., Lindbergh, G., Lagergren, C., 2014. Electrochemical performance of reversible molten carbonate fuel cells. International Journal of Hydrogen Energy 39, 12323–12329. doi:10.1016/j.ijhydene.2014.02.144

Ibrahim Dincer, 2012. Green methods for hydrogen production. International Journal of Hydrogen Energy 37, 1954–1971. doi:10.1016/j.ijhydene.2011.03.173

Laurencin, J., Mougin, J., 2015. High-Temperature Steam Electrolysis, in: Hydrogen Production. Wiley-VCH Verlag GmbH & Co. KGaA, Weinheim, Germany, pp. 191–272. doi:10.1002/9783527676507.ch6

Lovegrove, K., Stein, W., 2012. Concentrating solar power technology : principles, developments and applications. Woodhead Publishing.

Mazloomi, K., Sulaiman, N.B., Moayedi, H., 2012. Electrical Efficiency of Electrolytic Hydrogen Production. Int. J. Electrochem. Sci 7, 3314–3326.

Petipas, F., Brisse, A., Bouallou, C., 2013. Model-based behaviour of a high temperature electrolyser system operated at various loads. Journal of Power Sources 239, 584–595. doi:10.1016/j.jpowsour.2013.03.027

Sanz-Bermejo, J., Gallardo-Natividad, V., González-Aguilar, J., Romero, M., 2014a. Coupling of a Solid-Oxide cell unit and a linear Fresnel reflector field for grid management. Energy Procedia 57, 706–715. doi:10.1016/j.egypro.2014.10.226

Sanz-Bermejo, J., Muñoz-Antón, J., Gonzalez-Aguilar, J., Romero, M., 2015. Part load operation of a solid oxide electrolysis system for integration with renewable energy sources. International Journal of Hydrogen Energy 40, 8291–8303. doi:10.1016/j.ijhydene.2015.04.059

Sanz-Bermejo, J., Muñoz-Antón, J., Gonzalez-Aguilar, J., Romero, M., 2014b. Optimal integration of a solid-oxide electrolyser cell into a direct steam generation solar tower plant for zero-emission hydrogen production. Applied Energy 131, 238–247. doi:10.1016/j.apenergy.2014.06.028

Schiller, G., Ansar, A., Lang, M., Patz, O., 2009. High temperature water electrolysis using metal supported solid oxide electrolyser cells (SOEC). Journal of Applied Electrochemistry 39, 293–301. doi:10.1007/s10800-008-9672-6

Trnsys, 2007. TRNSYS 16: Volume 8 Programmer's Guide, in: Solar Energy Laboratory Univ. of Wisconsin-Madison (Ed.), TRNSYS 16 a TRaNsient SYstem Simulation Program.

Ulleberg, Ø., 2003. Modeling of advanced alkaline electrolyzers: A system simulation approach. International Journal of Hydrogen Energy 28, 21–33. doi:10.1016/S0360-3199(02)00033-2

Yu, L.J., Ren, G.P., Jiang, X.M., Yuan, J.Q., Cao, G.Y., 2007. Experiment and numerical simulation on the performance of a kw-scale molten carbonate fuel cell stack. Brazilian Journal of Chemical Engineering 24, 523–533. doi:10.1590/S0104-66322007000400006

Zeng, K., Zhang, D., 2009. Recent progress in alkaline water electrolysis for hydrogen production and applications. Progress in Energy and Combustion Science 36, 307–326. doi:10.1016/j.pecs.2009.11.002